Polymer 50 (2009) 4048–4055

Contents lists available at ScienceDirect

Polymer

journal homepage: www.elsevier.com/locate/polymer

Long-term creep of polyphenylene sulfide (PPS) subjected to complex thermal histories: The effects of nonisothermal physical aging

Yunlong Guo, Roger D. Bradshaw*

Department of Mechanical Engineering, J. B. Speed School of Engineering, University of Louisville, Louisville, KY 40292, USA

ARTICLE INFO

Article history:
Received 25 March 2009
Received in revised form
17 June 2009
Accepted 20 June 2009
Available online 26 June 2009

Keywords:
Long-term creep
Effective time
Nonisothermal physical aging

ABSTRACT

The long-term viscoelastic behavior of polymeric materials used below the glass transition temperature (T_g) is greatly affected by physical aging. In contrast to isothermal physical aging, long-term response under nonisothermal history has received far less attention. This paper reports experimental results and analytical methods of long-term creep behavior of polyphenylene sulfide (PPS) subjected to complex thermal histories in a temperature range below T_g. To characterize the effects of aging, creep tests were performed using a dynamic mechanical analyzer (DMA). Besides the long-term data, short-term creep tests in identical thermal conditions were also analyzed; these were utilized with effective time theory to predict long-term response under both isothermal and nonisothermal temperature histories. The long-term compliance after a series of temperature changes was predicted by the effective time theory using the KAHR-a_{te} model to obtain nonisothermal physical aging shift factors. Comparison of theoretical predictions with experimental data shows good agreement for various thermal histories.

1. Introduction

Long-term mechanical behavior of glassy polymers is a critical issue for many structural applications using polymer-based materials. During their service life, the viscoelastic properties of polymers can be strongly affected by physical aging, especially as temperatures approach the glass transition temperature T_g. Hence, the effects of physical aging on mechanical responses have received a great deal of attention in the past several decades [1–11]. Struik [12], McKenna [13], Tomlins [14] and other researchers [15–18] have used creep tests of neat polymers and polymeric matrix composites (PMCs) to experimentally determine the long term effects of physical aging. Effective time approaches, developed by Hopkins and Haugh [19,20], can also be used to predict long-term behavior from short-term tests. For example, Struik [12] has shown fairly good predictive capabilities for long-term creep response of PVC at constant temperatures.

In recent years, investigators put forward several models in order to describe long-term data with good accuracy for specific materials or applications. Read and Tomlins [21–23] used a stretched exponential function, combined with an equation of the relaxation time over wide ranges of aging time and loading time to represent long-term compliance; their numerical results provided reasonable predictions to long-term data on polypropylene and PVC. Arnold and White [24] compared the θ concept model and the so-called universal formula (Kohlrausch function) method (incorporated effective time theory) with long-term creep data in PMMA; they reported that the universal formula method produced a satisfactory fit, with the effects of aging being taken into account through the use of an effective time, while the θ concept model was not very successful. Skrypnyk and co-workers [25] introduced a constitutive model for long-term behavior of thermoplastics, which integrates effective time theory and a generalized Schapery model; for the material in their study, the model led to good long-term predictions for multi-step stress loading and recovery tests. Another constitutive model derived from the effective time concept was proposed by Zheng and Meng [26]. The authors claimed that this model is identical with classical effective time theory when the aging time is sufficiently long; however, at short times, the former is more suitable for chrono-rheologically simple materials since it can account for the transition to the asymptotic state. This model was used with PMC tests and the results matched the experimental findings.

Most investigations above have attempted to develop models based on the classical effective time theory; these approaches have been largely focused on improving predictive abilities or calculating the long-term response for specific materials at constant or varying stress levels. It is a remarkable fact that all of research on long-term viscoelastic response of polymers in the literature is conducted at isothermal conditions; this means that the material is

* Corresponding author. Tel.: +1 502 852 6099; fax: +1 502 852 6053.
E-mail address: roger.bradshaw@louisville.edu (R.D. Bradshaw).

0032-3861/$ – see front matter © 2009 Elsevier Ltd. All rights reserved.
doi:10.1016/j.polymer.2009.06.046

quenched from a temperature above the glass transition temperature (T_g) to an test temperature $T < T_g$ and held at this temperature until the long-term test is complete. While isothermal long-term physical aging has been extensively studied, long-term mechanical properties with physical aging effects after a varying temperature history has received far less scrutiny.

Since structures built using PMCs often undergo complicated temperature changes in their applications for long periods, it is necessary to develop techniques for describing and predicting long-term effect of nonisothermal physical aging on such polymeric materials. In this paper, we address the nonisothermal long-term creep response and provide a prediction method for glassy polymers. Experimental methodology is presented first followed by the introduction of KAHR-a_{te} model and the extended effective time theory for multi-step temperature conditions. Testing results and comparison with the model predictions are subsequently illustrated for PPS film; the results agree well with the presented model. While this paper presents results for pure polymers, it is anticipated that this approach would also be suitable for PMCs in which the polymer matrix, subjected to physical aging effects, is reinforced by an elastic phase (such as carbon or glass fibers).

2. Experimental

2.1. Materials and test equipment

The material chosen for this study is 0.127 mm (5 mil) thick PPS film (SUPEC® PPS RESIN) supplied by GE Advanced Materials as 280 mm by 216 mm sample sheets. Experimental specimens were cut manually to be 25.4 mm long (in the load direction) and 12.7 mm wide. The PPS films are in semi-crystalline state as received. Previous studies have shown that physical aging in semi-crystalline polymers can occur on wide temperature ranges and have a particularly impact on polymeric products [27–30]. Semi-crystalline PPS has increasing applications in automotive, coatings, electrical, electronics industry at high temperature over a prolonged period of time. Consequently, physical aging can exert a significant influence on the long-term mechanical properties of such PPS products [31]. It should be noted that the temperatures used in this study ($T_g + 5$ °C and below) are well below the melting temperature of the PPS films; in this case, past research suggests that the crystalline phase will remain unchanged [32] although this has not been demonstrated by the authors in the current work. The amorphous phase of the PPS film is subject to physical aging effects below T_g, however; it is the change in polymer mechanical behavior due to these effects that is observed in this study.

Uniaxial tension load was applied in the long direction during creep tests. The value of T_g reported by the manufacturer for the PPS film is 92 °C; this value is consistent with observations by the authors via the tan δ (loss factor) peak using an RSA3 DMA in tension tests [33]. The long-term creep tests reported in this paper are also performed on this equipment.

2.2. Nonisothermal long-term creep

This paper investigates long-term viscoelastic properties after complicated thermal histories (more than one temperature jump after quenching from $T > T_g$). In the current study, the material is first headed to 5 °C above T_g and held for 5 min to erase internal stresses (rejuvenation)[1]. The material is then quenched to $T < T_g$ to place the material in the glassy state; for the remainder of the experiment, the temperature varies in the range from $T_g - 65$ °C to $T_g - 15$ °C via a series of temperature changes, including up-jumps and down-jumps, in order to achieve complicated thermal histories.

At the final temperature in the thermal history, characterization of the aging state occurs using long-term creep and recovery test. All creep tests begin 0.5 h from the instant at which the specimen has first reached the final temperature. Creep tests are performed in tension and generally last for at least 10 h; test details will be presented in the next section.

The thermal histories of PPS film considered in this paper include:

97 °C (5 °C above T_g) → 57 °C (14 h) → 73 °C
97 °C → 63 °C (14 h) → 73 °C
97 °C → 57 °C (10 h) → 67 °C (4 h) → 73 °C
97 °C → 67 °C (4 h) → 77 °C (10 h) → 73 °C
97 °C → 27 °C (12 h) → 73 °C (1 h) → 27 °C (1 h) → 73 °C
97 °C → 57 °C (4 h) → 73 °C (6 h) → 67 °C

The thermal histories above are chosen based the following considerations:

(1) Representativeness. The temperature histories include both up-jumps and down-jumps and consist of one-step, two-step and three-step temperature changes after quenching in order to form various nonisothermal conditions. The authors believe this combination captures to some extent the variations that might be experienced by structures in service.
(2) Temperature range. The temperatures in these thermal histories varied between room temperature (27 °C) and 15 °C below T_g; for most of the tests, the temperature is not far from glass transition temperature (15–35 °C below T_g) to allow the material's aging state to change sufficiently in the lab time scale (~14 h for thermal treatment). Excursions to room temperature provide some consideration of the effect of aging time spent relatively far from equilibrium.
(3) Creep test temperatures. All creep tests are performed at a final temperature of 73 °C or 67 °C; these were chosen since previous work by the authors has characterized the isothermal physical aging behavior of PPS. [33] Fig. 8 of this work provides the basis to compare long-term response under isothermal and nonisothermal conditions.

The authors believe that these thermal histories are reasonable for use as multiple-step temperature changes in glassy state for the purpose of examining the KAHR-ate model capabilities for data prediction. It must be noted that these represent only one set of possible choices among the infinity of possibilities that could be selected. However, based on the agreement between the data and the model presented below, the authors believe other similar temperature histories would lead to similar outcomes using the KAHR-a_{te} model.

After the thermal histories described are applied, long-term creep tests are conducted at the final temperature attained (either 73 °C or 67 °C). It should be emphasized that long-term in this context means that the load duration is such that the aging state changes appreciably during the loading history (i.e. the creep tests do not consist of short-term load steps during which the aging shift factor remains approximately constant). One obvious difference from isothermal creep is that the definition of the "aging time" is no longer clear; in this paper, it is defined as the time elapsed since the step to the final temperature instead of the time elapsed since quenching from above T_g. The stress level applied to the specimens (4.87 MPa) remains in the linear viscoelastic regions at 73 °C and

[1] At temperature above T_g, the amorphous portion in PPS material establishes thermodynamic equilibrium, while the crystalline portion remains crystalline.

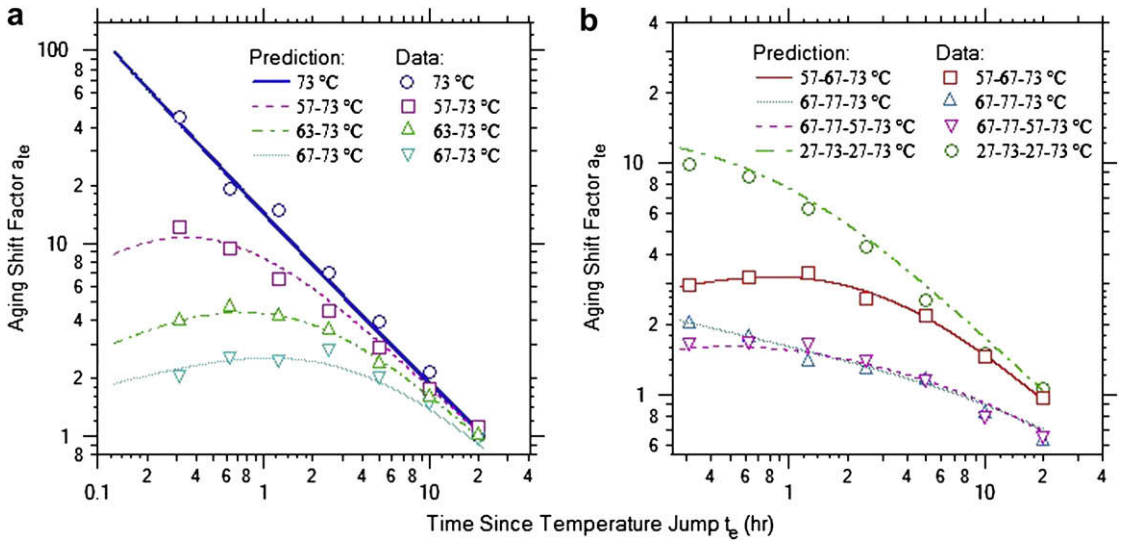

Fig. 1. Prediction of mechanical aging shift factor by KAHR-a_{te} model for various thermal histories: (a) single temperature up jump and isothermal 73 °C; (b) multiple temperature jumps. Experimental data are the average of three data sets of sequenced creep experiments and reference curve for nonisothermal aging shift factors is the isothermal compliance response at 73 °C with aging time = 20 h.

67 °C; details on determining linear ranges are presented elsewhere [33].

3. Effective time theory

3.1. Aging shift factors and KAHR-a_{te} model

Effective time theory describes long-term compliance via the short-term creep response momentary master curve (MMC) and aging shift factors a_{te}; these relate the short-term compliance in the aged state to that of the reference state as $D(t)|_{t_e} = D_{ref}(a_{te}t)|_{t_{eref}}$. Similarly, the nonisothermal aging shift factors a_{te} from short-term tests need to be known in order to obtain the effective time for the multi-step temperature histories. The KAHR-a_{te} model, developed by the authors [34,35], combines the KAHR [36] model of volume recovery with a suitable linear relationship between aging shift factors and structural shift factor regarding specific volume:

$$a_{te}(a_\delta)|_T = \left(\frac{c_0}{a_\delta}\right)^{c_1};\ c_0, c_1 > 0 \tag{1}$$

where T is the temperature of mechanical loading, c_0 and c_1 are temperature dependent constants, a_{te} is physical aging shift factor, and a_δ is the structural shift factor defined in the KAHR model.

In the KAHR model, the volume recovery behavior can be expressed by the normalized departure from equilibrium δ, which is defined by:

$$\delta(t,T) = \frac{v(t) - v_\infty(T)}{v_\infty(T)} \tag{2}$$

where v and v_∞ are instantaneous and equilibrium specific volume, respectively. The volume response is defined in terms of the reduced time z as:

$$\delta(z) = -\Delta\alpha \int_0^z R(z-\varsigma)\frac{dT}{d\varsigma}d\varsigma;\ z = \int_0^t \frac{d\xi}{a_T a_\delta};\ R(z) = e^{-(z/\tilde{\tau})^{\tilde{\beta}}} \tag{3}$$

where $\Delta\alpha = \alpha_l - \alpha_g$ is the difference in coefficient of thermal expansion between the liquid and glassy state, in this work, it is $4.0\times10^{-4}\,K^{-1}$ [33], T is temperature, $R(z)$ is a normalized retardation function (in this case expressed as a Kohlrausch stretched exponential function using $\tilde{\tau}$ and $\tilde{\beta}$), a_T is the temperature shift factor, and a_δ is the structural shift factor.

The shift factors a_T and a_δ follow the exponential forms suggested by the KAHR model [36] and later modified by Schultheisz et al. [37] as:

$$a_T = \exp\left[-\Delta\alpha\zeta e^b(T - T_r)\right];\ a_\delta = \exp(-\zeta\delta);\ e^{-b} = 1 - x;$$
$$\zeta = \frac{(1-x)\theta}{\Delta\alpha} \tag{4}$$

where T_r is a reference temperature, θ is a material constant, x is a partition parameter ($0 \le x \le 1$), b and ζ are material constants, introduced to simplify the solution in the case of $T = T_r$ (i.e. a_T is fixed at unity and a_δ is relevant to a single parameter ζ). This model has been used successfully to predict specific volume response of glassy polymers under a variety of temperature histories [36,38,39].

The KAHR-a_{te} model can be utilized to predict aging response or to determine necessary model parameters from a set of aging shift factor data. Fig. 1 depicts experimental data and horizontal aging shift factor predictions from the KAHR-a_{te} model over various thermal histories [34,40,41]. The model parameters, listed in Table 1, were identified from the three single-step temperature up jump tests in Fig. 1(a); comparison of model predictions and testing results on some extra temperature scenarios, including most thermal histories for long-term creep in this paper, is shown in Fig. 1(b). Slight vertical shifting (within ±5%) was applied on the reference curve (see the caption of Fig. 1) before calculating horizontal aging shift factors. It is clear that the KAHR-a_{te} model

Table 1
KAHR-a_{te} model parameters for PPS.

Parameter	ζ (unitless)	b (unitless)	θ (K^{-1})	c_0 (unitless)	c_1 (unitless)	$\tilde{\tau}$ (s)	β (unitless)
Value	253.817	0.919	0.255	0.633	12.422	477.289	0.092

successfully characterizes nonisothermal physical aging after several temperature jumps. Since the model coefficients were determined from a series of single temperature jump histories, this work demonstrates that the KAHR-a_{te} model has the capacity of predicting material response for more complicated thermal conditions. Details regarding this model are available in our previous publications [34,40].

3.2. Effective time of nonisothermal aging

3.2.1. Effective time theory

Consider an isothermal aging creep test with an initial aging time of t_e^0. At a later moment in the test, the aging time will be $t_e^0 + t$, where t is the time elapsed from load initiation (stress or strain, corresponding to creep or stress relaxation, respectively). When the testing time t approaches and exceeds the value of the initial aging timet_e^0, one would expect deviation of the long-term creep/stress relaxation response from the momentary (i.e. short-term) response due to the change in the material aging state. Taking the initial aging time t_e^0 to be the reference aging time ($t_{eref} = t_e^0$) of the MMC, the shift factor at any instant in time can be defined based on the shift rate μ [12]:

$$a_{te}^0(t) = \left(\frac{t_e^0}{t_e^0 + t}\right)^{\mu} \tag{5}$$

To account for the cumulative effects of aging, the effective time increment $d\lambda$ corresponding to a real time increment dt is then defined:

$$d\lambda = a_{te}^0(t)dt \tag{6}$$

By integration, the total test time can be related to the effective time, $\lambda(t)$:

$$\lambda(t) = \int_0^t a_{te}^0(\xi)d\xi \tag{7}$$

Using the effective time in place of real time in the Kohlrausch function

$$D(t) = D_0 e^{(\lambda/\tau)^{\beta}} \tag{8}$$

results in a prediction of long-term creep response, where D_0 is initial compliance, τ is the relaxation time, and β is the stretch parameter of the MMC at $t_e^0 = t_{eref}$.

In isothermal physical aging, the shift rate is defined as $\mu = -d\log a_{te}/d\log t_e$; this reflects the fact that the shift factors a_{te} versus t_e form a straight line in log-log space (Fig. 1(a)). However, in nonisothermal cases, the plot of log a_{te} with log t_e is no longer a line, thus the shift rate is not constant but a function of time (Fig. 1). Bradshaw and Brinson [42] introduced the concept of "effective aging time" to account for the nonlinear aging effects following a temperature jump. In their work, continuous aging shift factor information under single temperature up-jump or down-jump condition was exacted using effective time theory. This method might be used to predict long-term response for non-isothermal aging.

In current paper, an alternate approach is considered. During nonisothermal physical aging, aging shift rate is denoted as $\mu^*(\xi)$, the effective time $\lambda^*(t)$ is given by:

$$a_{te} = \left(\frac{t_e^0}{t_e^0 + t}\right)^{\mu^*(\xi)} \rightarrow \lambda^*(t) = \int_0^t \left(\frac{t_e^0}{t_e^0 + \xi}\right)^{\mu^*(\xi)} d\xi \tag{9}$$

Note that $\mu^*(\xi)$ should approach the isothermal shift rate μ of the final temperature if time is long enough since the last temperature jump.

3.2.2. Determination of μ^* and λ^*

In order to create long-term predictions, the effective time $\lambda^*(t)$ must first be obtained from a given shift factor data set obtained from either a nonisothermal physical aging test or from KAHR model predictions. One approach to determine λ^* would be to evaluate the integral in Eq. (7) directly, using either a_{te} data points (approximated by a suitable, integrable function) or KAHR-a_{te} predictions of a_{te}. Alternately, the nonisothermal aging shift rate μ^* could first be evaluated based upon the a_{te} data/prediction and then utilized in Eq. (9). Both approaches lead to similar results; findings utilizing the aging shift rate μ^* are considered to below to highlight one aspect of the long-term test results.

The aging shift rate can be written by:

$$\mu^*(t_e) = -\frac{d\log a_{te}}{d\log t_e};\ t_e = t_e^0 + t \tag{10}$$

where t_e is the nonisothermal aging time, defined as the time elapsed since last temperature jump, t_e^0 is initial aging time when a long-term creep test starts, t is the loading time of the creep test. Note that the shift rate μ^* after multiple temperature jumps is a function of the test time t in long-term experiments. If the test time t is long enough, μ^* at a distant time after the changes of temperature should approach the isothermal shift rate μ_{iso} of the test temperature; this is equivalent to the "fading memory" concept, in which the material held at a single temperature long after various temperature steps begins to act as though it were only subjected to isothermal physical aging. Consequently, μ^* can be separated into two parts as $\mu^*(t) = \mu_{iso} + \tilde{\mu}(t)$, where $\tilde{\mu}(t)$ represents the difference of aging shift rate in isothermal and nonisothermal conditions.

The shift rate function $\mu^*(t_e)$ can be obtained from the predicted aging shift factors or experimental data. In this study, KAHR-a_{te} predictions are used to determine shift rates after various temperature histories. Once the numerical values of shift rate are attained by Eq. (10), suitable curves are chosen to fit the shift rate values over the loading time of creep tests for most thermal history cases. Fig. 2 demonstrates aging shift rates for several nonisothermal cases right after the material reaching the final temperature (73 °C).

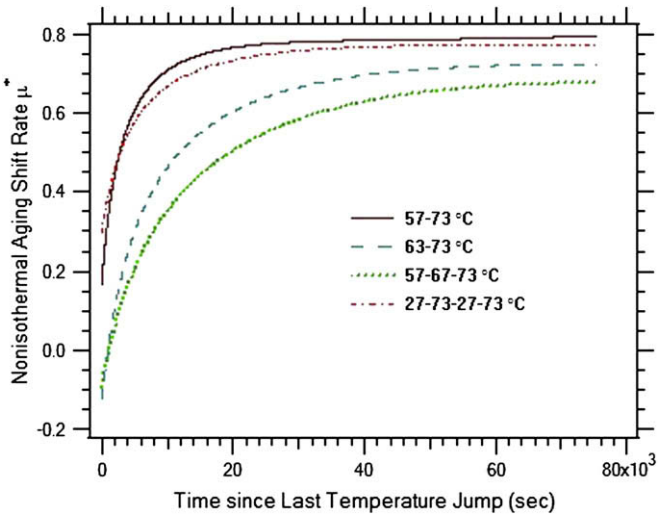

Fig. 2. Nonisothermal aging shift rate μ^* for complex thermal histories, values of $\mu^*$are calculated using the predicted a_{te} from KAHR-a_{te} model.

Once suitable functions for μ^* are obtained, the effective time was calculated using a MATLAB program. Effective time curves versus real time for several thermal histories are shown in Fig. 3. When the effective time has been evaluated, the long-term creep response subjected complicated thermal history can be predicted by Eq. (8).

4. Results and discussion

4.1. Long-term creep results of nonisothermal aging

Figs. 4 and 5 depict long term creep responses for four thermal histories. For each thermal history, test results from three replicates are plotted. The creep tests last for at least 10 h, while the aging time since last temperature jump is 0.5 h. It is clear that the long-term creep compliance curves are consistent with each other under the same experimental condition; the maximum deviation of compliance values between any individual data set and the average was found less than 5%, while the average deviation is less than 2%.

The long-term creep data were collected in two successive time zones. The first time zone covers the time scale from the starting of loading ($t=0$) to $t=180$ s and the second time zone is the remainder of total loading time. Note that the creep data are evenly distributed in real time; this is the reason that in Figs. 4 and 5, one sees more data points near the ends of both time zones (x axis is in logarithmic scale). The data collected in time zone 1 is considered as the short-term response of creep ($t/t_e \leq 0.1$) [1,3,21,22]; this data is utilized by the nonisothermal effective time theory for predicting the long-term response. The whole data set of compliance curve represents the long-term response of nonisothermal physical aging; it will be compared with numerical results to validate the effective time theory under complicated thermal histories.

4.2. Prediction of nonisothermal long-term creep behavior

4.2.1. Predictions for various complicated thermal histories

Once the effective time λ^* has been calculated, it can be used to predict long-term response of a polymer during nonisothermal physical aging. From the short-term creep test results

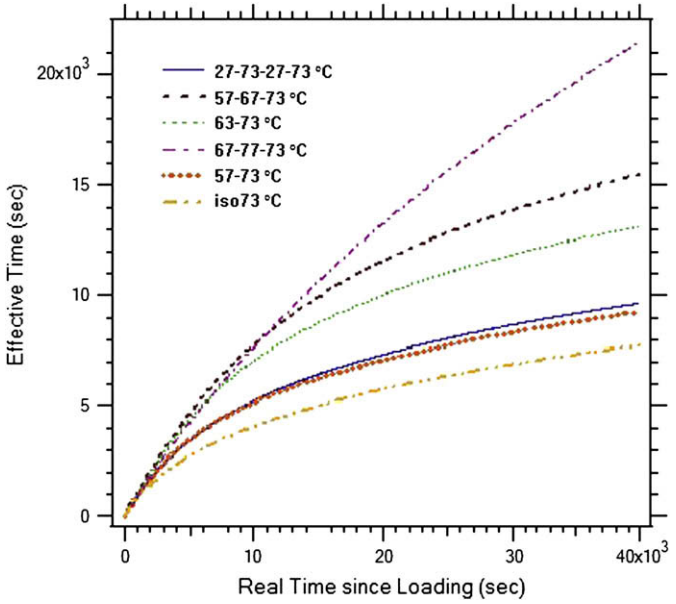

Fig. 3. Calculated effective time for several isothermal and nonisothermal conditions.

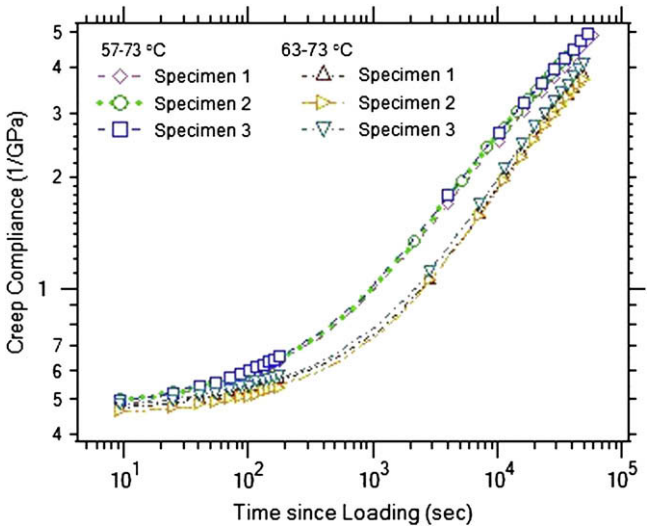

Fig. 4. Long-term creep compliance curves of two thermal histories: 97 °C → 57 °C → 73 °C and 97 °C → 63 °C → 73 °C.

demonstrated above (compliance in time zone 1), Kohlrausch function parameters D_0, τ and β were identified. Using these parameters and effective time λ^* in Eq. (8), the long-term compliance prediction is obtained. Figs. 6 and 7 illustrate compliance predictions for long-term creep by using Kohlrausch function (Eq. (8)). Parameters D_0, τ and β from the short-term data are listed in Table 2. For the purpose of comparison, Kohlrausch functions in the effective time and real time domain are shown in these two figures. It is clear that the model predictions based effective time theory lead to good agreement with our experimental findings in all of the thermal histories considered. The results from original Kohlrausch equation, which capture short time response very well, depart from the experimental data when the loading time is long enough. (i.e. $t_e^0 + t \gg t_e^0$)

In order to predict the long-term creep behavior after a nonisothermal temperature history, one needs to first perform a short-term test under the identical thermal condition and then obtain Kohlrausch function parameters of the short-term compliance curve. The aging shift factors a_{te} in the duration of long-term test

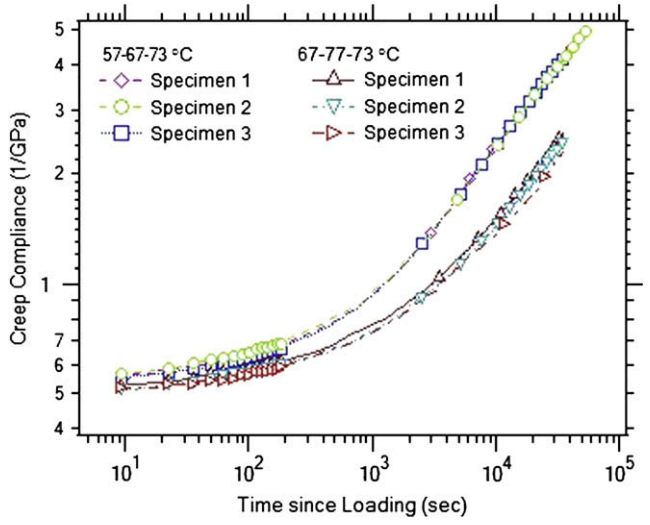

Fig. 5. Long-term creep compliance curves of two thermal histories: 97 °C → 57 °C → 67 °C → 73 °C and 97 °C → 67 °C → 77 °C → 73 °C.

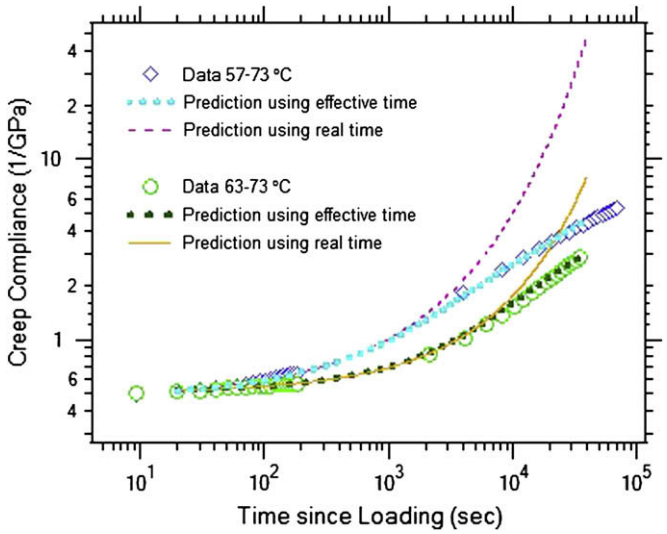

Fig. 6. Long-term creep predictions by effective time theory and original Kohlrausch function from short-term response; thermal histories: 97 °C → 57 °C → 73 °C and 97 °C → 63 °C → 73 °C.

are predicted by the KAHR-a_{te} model using parameters in Table 1. These a_{te} are with Eqs. (9) and (10) to calculate effective time λ^*. The long-term compliance is finally predicted by Eq. (8) by inserting λ^* and Kohlrausch function parameters D_0, τ and β from the short-term test.

Fig. 8 depicts the prediction and data for a more complicated thermal treatment: 97 °C → 27 °C (12 h) → 73 °C (1 h) → 27 °C (1 h) → 73 °C. In this test, the specimen experienced temperature changes in a wide range; and the creep duration was 100 h. The aim for this investigation is to examine the capacities of nonisothermal effective time theory when the creep process is rather long, subjected to elevated varying thermal circumstances. As in Figs. 6 and 7, the predictions made using the unaged Kohlrausch function and with nonisothermal effective time theory using the KAHR-a_{te} model are plotted in Fig. 8; good agreement is obtained between the data and the KAHR-a_{te} model prediction. In order to demonstrate the importance of properly assessing the aging state, Fig. 8 also contains

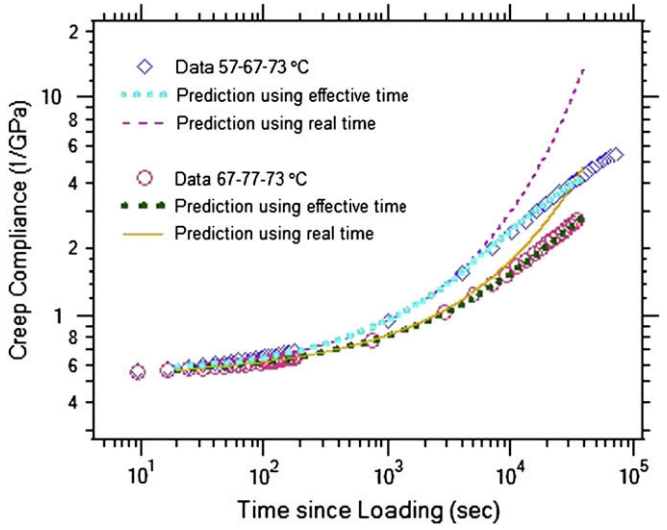

Fig. 7. Long-term creep predictions by effective time theory and original Kohlrausch function from short-term response; thermal histories: 97 °C → 57 °C → 67 °C → 73 °C and 97 °C → 67 °C → 77 °C → 73 °C.

Table 2
Parameters of Kohlrausch function to fit short-term creep response.

Thermal history	D_0 (1/GPa)	τ (s)	β (unitless)
97 °C → 57 °C → 73 °C	0.453	1603	0.478
97 °C → 63 °C → 73 °C	0.461	3287	0.523
97 °C → 57 °C → 67 °C → 73 °C	0.528	3176	0.469
97 °C → 67 °C → 77 °C → 73 °C	0.523	6463	0.437

a prediction using effective time theory under isothermal conditions (i.e. Eqs. (5) and (7) using the isothermal shift rate). In a previous publication [27], we identified the (isothermal) shift rate $\mu = 0.811$ via isothermal creep tests at 73 °C. As Fig. 8 clearly demonstrates, the predictions using isothermal effective time theory overestimates the creep compliance after 1300 s since loading and is in significant disagreement with test data by the end of the test (more than 100% error). This indicates that isothermal physical aging approaches cannot be used to predict nonisothermal physical aging test data without significant modification. On the other hand, the numerical result utilizing the KAHR-a_{te} model matches the experimental finding fairly well, with errors at 10 and 100 h since loading being 5.1% and 12.9%, respectively. Consider that the prediction is made by using the information from the first 180 s of this creep test and aging shift factors from KAHR-a_{te} calculation, this example shows good predictive abilities of nonisothermal effective time theory.

4.2.2. Predictions with different final temperatures

The long-term creep properties discussed so far were examined at a single temperature (73 °C) after multiple temperature steps; this is because the KAHR-a_{te} model parameters were developed from tests at 73 °C following various thermal histories. Although the model parameters were determined by single step temperature up jumps with the identical final temperature, it is possible to extend the predictive ability of KAHR-a_{te} model to final temperatures other than 73 °C.

In order to accomplish this, a temperature shift factor $a_{T,\delta}$ must be introduced to allow parameters c_0 and c_1 to relate the predicted a_δ with the aging shift factors a_{te} at another temperature. The reason is that the reference curve of a_{te} is currently defined on the non-equilibrium state of polymers, at a particular aging time and

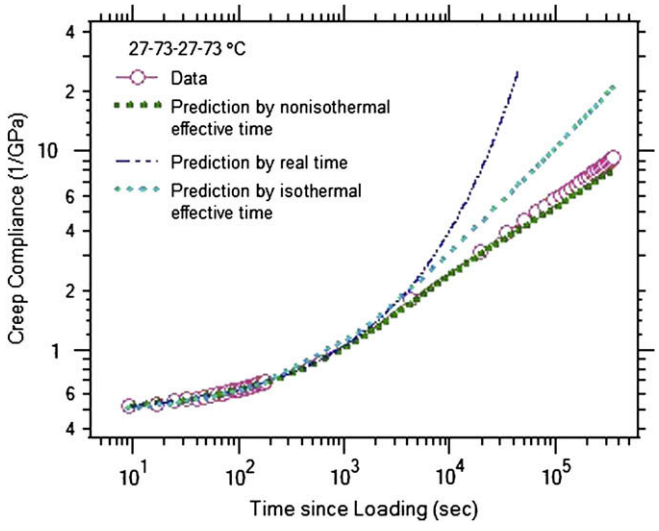

Fig. 8. Long-term creep predictions by isothermal and nonisothermal effective time theory and original Kohlrausch function from short-term response; thermal histories: 97 °C → 27 °C → 73 °C → 27 °C → 73 °C. Kohlrausch function parameters: $D_0 = 0.460$ GPa^{-1}, $\tau = 1593$ s, $\beta = 0.417$.

a particular temperature; in other words, the reference curves for a_{te} depend on thermal histories while the temperature shift factor a_T and structural shift factor a_δ in the KAHR model are defined to link the retardation time at a reference temperature T_r in equilibrium ($\delta = 0$) to the retardation time at temperature T, and $\delta \neq 0$. This significant difference requires a shift factor, $a_{T,\delta}$, which scales a_δ at the reference aging times from current temperature to the reference temperature, in order to use the model parameters obtained from the reference temperature to predict material response at different temperatures.

As described above, $a_{T,\delta}$ is defined as:

$$a_{T,\delta} = a_{\delta,\mathrm{iso}}\left(T_r, t_{\mathrm{eref}}\right) \Big/ a_{\delta,\mathrm{iso}}\left(T, t_{\mathrm{eref}}\right) \tag{11}$$

where the $a_{\delta,\mathrm{iso}}(T_r, t_{\mathrm{eref}}))$ is the isothermal structural shift factor at the reference aging time t_{eref} at temperature T_r, the temperature at which the model parameters were identified. Similarly, $a_{\delta,\mathrm{iso}}(T, t_{\mathrm{eref}})$ is the isothermal structural shift factor at the reference aging time at temperature T. Thus, the correlation of a_{te} and a_δ is:

$$a_{te}(a_\delta)|_T = \left(\frac{c_0}{a_\delta a_{T,\delta}}\right)^{c_1}; \text{ constants } c_0, c_1 > 0 \tag{12}$$

The KAHR-a_{te} model maps structural shift factor a_δ to aging shift factor a_{te} by parameters c_0 and c_1 at the reference temperature. The aging temperature factor $a_{T,\delta}$ couples predicted a_δ and a_{te} for the reference curves at other temperatures and therefore enables the model to predict aging shift factors in wider temperature ranges. As proposed in Eq. (12), the KAHR-a_{te} model assumes parallel linear relationships between a_δ and a_{te} in log-log space for different final temperatures below T_g, with parameter c_1 being the slope of these straight lines and $c_0/a_{T,\delta}$ representing the intercept . Eqs. (11) and (12) are applied to predict viscoelastic response at 67 °C for PPS. Fig. 9 shows the experimental data and prediction of a_{te} on thermal history 97 °C → 57 °C → 73 °C → 67 °C, model parameters are listed in Table 1. The structural shift factor at reference aging time on 67 °C $a_\delta(67^\circ\mathrm{C}, t_e = 72{,}000\ \mathrm{s})$ is equal to 0.5673; similarly, the reference structural shift factor on reference temperature $a_\delta(73^\circ\mathrm{C}, 72{,}000\ \mathrm{s}) = 0.6300$. Therefore, $a_{T,\delta} = 0.5673/0.6300 = 0.9005$. As seen in Fig. 9, the model involving the temperature shift factor results in excellent prediction, validated by

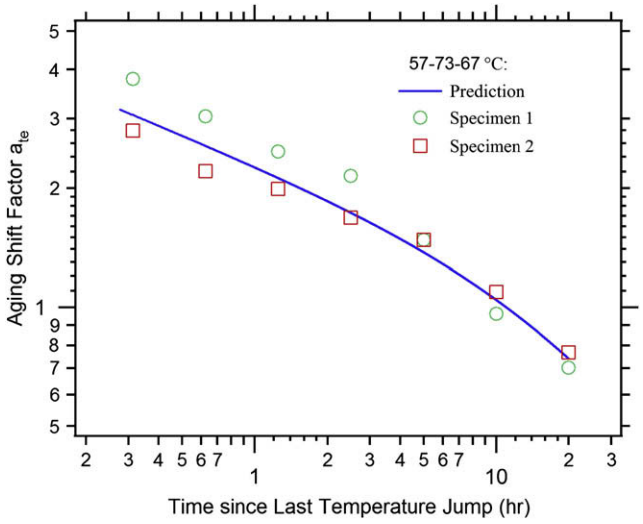

Fig. 9. Prediction of mechanical aging shift factor by KAHR-a_{te} model for thermal history: 97 °C → 57 °C (4 h) → 73 °C (6 h) → 67 °C. Reference curve is the isothermal compliance response at 67 °C with aging time = 20 h.

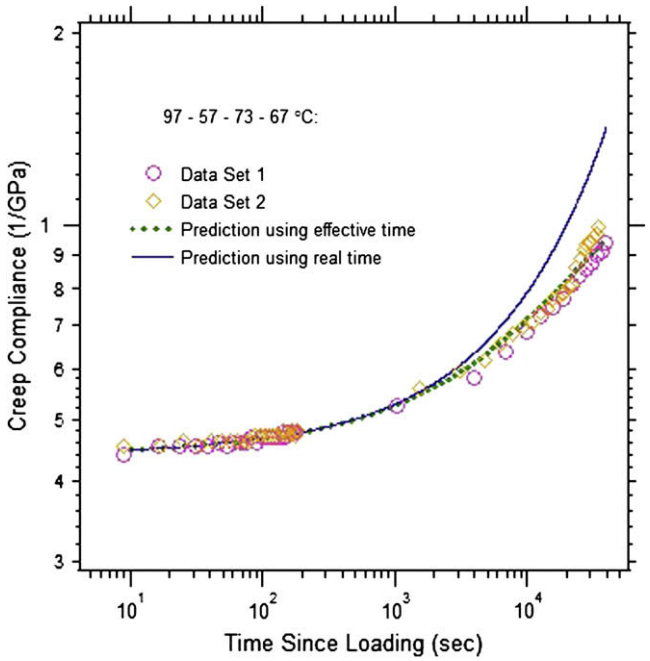

Fig. 10. Long-term creep predictions by nonisothermal effective time theory and original Kohlrausch function from short-term response; the thermal history is: 97 °C → 57 °C → 73 °C → 67 °C. Kohlrausch function parameters: $D_0 = 0.432\ \mathrm{GPa}^{-1}$, $\tau = 48929$ s, $\beta = 0.410$.

our experiments on the specific thermal history with the final temperature different, but not far away from 73 °C.

Nonisothermal effective time based on predicted aging shift factors in Fig. 9 for this thermal treatment was calculated for the long-term creep starting from 0.5 h after reaching the final temperature (67 °C). The long-term creep data sets and prediction by effective time theory are illustrated in Fig. 10 with the associated Kohlrausch short-term fit parameters listed in the caption. The resulting long-term predictions are compared with the material responses found in two experiments using different samples. Due to the data scatter among individual tests revealed in previous section, the second data set in Fig. 10 was shifted vertically by the amount of 4.5% prior to comparison to bring the short-term behavior in line for both data sets.

These results demonstrate good agreement between nonisothermal effective time theory and long-term creep response data after multiple-step temperature histories. Note that the KAHR-a_{te} model plays a key role in modeling long-term viscoelastic properties, since it describes isothermal and nonisothermal aging shift factors, which are the basis for the calculation of effective time.

Although the prediction on the thermal history 97 °C → 57 °C → 73 °C → 67 °C match the experimental findings quite well, this should not be interpreted as meaning that the model can provide reliable results to arbitrary thermal histories ending at any temperature. The example shown in Fig. 10 indicates the theory is applicable when the final temperature is not far from the reference temperature at which the model parameters are identified; moreover, Eqs. (11) and (12) need to be examined in a wider temperature range in future work to better understand the limitations of this approach.

5. Conclusions

Several complex thermal histories have been applied to PPS films. After these thermal treatments, long-term creep tests are performed using a DMA to obtain the material response of due to

physical aging. Effective time theory along with the KAHR-a_{te} model using parameters obtained in earlier studies were applied to predict long-term creep response after multi-step temperature jumps. The results show clearly that the nonisothermal effective time theory successfully characterizes long-term mechanical behavior during physical aging. As such, it is anticipated that this approach can be used to successfully model the long-term physical aging response of PMCs under nonisothermal service temperature histories.

Acknowledgements

The authors would like to recognize Kentucky Science and Engineering Foundation (KSEF) for sponsorship of this work under the grant entitled KSEF-148-502-05-136, and Mr. Scott Cione, GE Advanced Materials, for supplying the materials used in this study.

Appendix A. Nonisothermal aging shift rate μ^* and effective aging time t_e^{eff} approaches

As mentioned in the text, Bradshaw and Brinson considered nonisothermal physical aging effects in terms of an "effective aging time" denoted as t_e^{eff} [37]. In this approach, the isothermal shift rate μ is used to evaluate the effective time, with the shift factor at a given moment in time determined using

$$a_{te} = \left(\frac{t_e^0}{t_e^{eff}}\right)^{\mu} \tag{A-1}$$

In this case, the effective aging time is expressed as a known function in terms of real (experiment) time. In the current paper, the aging shift rate μ^* has been defined to express the shift factor at a given time $t_{e0}+t$ since the most recent temperature jump as:

$$a_{te} = \left(\frac{t_e^0}{t_e^0+t}\right)^{\mu^*} \tag{A-2}$$

This assumes that the reference aging time is equal to the time at which the load is first applied (i.e. $t_{eref} = t_e^0$).

It is clear that a relationship between t_e^{eff} and μ^* exists. Setting the shift factor Eqs. (A-1) and (A-2) equal and raising both sides to the power $1/\mu$ leads to:

$$\left[\left(\frac{t_e^0}{t_e^{eff}}\right)^{\mu}\right]^{1/\mu} = \left[\left(\frac{t_e^0}{t_e^0+t}\right)^{\mu^*}\right]^{1/\mu} \tag{A-3}$$

Simplifying, the effective aging time t_e^{eff} and the aging shift rate μ^* are thus related as:

$$t_e^{eff} = t_e^0\left(\frac{t_e^0+t}{t_e^0}\right)^{\mu^*/\mu} \tag{A-4}$$

References

[1] Cizmecioglu M, Fedors RF, Hong SD, Moacanin J. Polym Eng Sci 1981; 21(14):940–2.
[2] Drozdov AD, Dorfmann A. Math Comput Modell 2003;37(7–8):665–81.
[3] Kemmish DJ, Hay JN. Polymer 1985;26(6):905–12.
[4] Matsumoto DS. Polym Eng Sci 1988;28(20):1313–7.
[5] O'Connell PA, McKenna GB. Polym Eng Sci 1997;37(9):1485–95.
[6] Read BE. J Rheol 1992;36(81):1719–36.
[7] Schwarzl FR, Kaschta J. Mech Time-Depend Mater 1998;2(1):13–36.
[8] Bradshaw RD, Brinson LC. Polym Eng Sci 1997;37(1):31–44.
[9] Bradshaw RD, Brinson LC. Mech Time-Depend Mater 1997;1(1):85–108.
[10] Spinu I, McKenna GB. Polym Eng Sci 1994;34(24):1808–14.
[11] Spinu I, McKenna GB. J Plast Film Sheeting 1997;13(4):311–26.
[12] Struik LCE. Physical aging in amorphous polymers and other materials. Amsterdam: Elsevier; 1978 [chapters 4, 10, and 11].
[13] McKenna GB, Leterrier Y, Schultheisz CR. Polym Eng Sci 1995;35(5):403–10.
[14] Tomlins PE, Read BE, Dean GD. Polymer 1994;35(20):4376–81.
[15] Miyano Y, Nakada M, Kasamori M, Muki R. Mech Time-Depend Mat 2000; 4(1):9–20.
[16] Gates TS, Feldman M. J Compos Technol Res 1995;17(1):33–42.
[17] Gates TS, Veazie DR, Brinson LC. J Polym Res 1997;31(24):2478–505.
[18] Brinson LC, Gates TS. Int J Solids Struct 1995;32(6–7):827–46.
[19] Hopkins IL. J Polym Sci 1958;28(118):631–3.
[20] Haugh EF. J Appl Polym Sci 1959;1(2):144–9.
[21] Tomlins PE, Read BE. Polymer 1998;39(2):355–67.
[22] Tomlins PE. Polymer 1996;37(17):4617–28.
[23] Read BE, Tomlins PE. Polymer 1997;38(18):4617–28.
[24] Arnold JC, White VE. Mater Sci Eng A 1995;197(2):251–60.
[25] Skrypnyk ID, Spoormaker JL, Kandachar P. In: Schapery RA, Sun CT, editors. Time dependent and nonlinear effects in polymers and composites. West Conshohocken: American Society for Testing and Materials; 2000. p. 71–82.
[26] Zheng SF, Weng GJ. Eur J Mech A-Solid 2002;21(3):411–21.
[27] Struik LCE. Polymer 1987;28(9):1521–33.
[28] Struik LCE. Polymer 1987;28(9):1534–42.
[29] Struik LCE. Polymer 1989;30(5):799–814.
[30] Struik LCE. Polymer 1989;30(5):815–30.
[31] Krishnaswamy RK, Geibel JF, Lewis BJ. Macromolecules 2003;36(8):2907–14.
[32] Aklonis JJ, MacKnight WJ. Introduction to polymer viscoelasticity, 2nd ed. New York: John Wiley and Sons; 1983. p. 42.
[33] Guo Y, Bradshaw RD. Mech Time-Depend Mat 2007;11(1):61–89.
[34] Guo Y, Wang N, Bradshaw RD, Brinson LC. J Polym Sci B: Polym Phys 2009;47(3):340–52.
[35] Bradshaw. Ph.D. dissertation, Northwestern University: Evanston, IL; 1997 (chapter 4).
[36] Kovacs AJ, Aklonis JJ, Hutchinson JM, Ramos AR. J Polym Sci: Polym Phys Ed 1979;17(7):1097–162.
[37] Schultheisz CR, McKenna GB, Leterrier Y, Stefanis E. SEM conference on experimental mechanics; 1995. p. 329–35.
[38] Ramos AR, Hutchinson JM, Kovacs AJ. J Polym Sci Part B Polym Phys 1984; 22(9):1655–96.
[39] Kovacs AJ. Ann NY Acad Sci 1981;371(10):38–66.
[40] Guo Y, Bradshaw RD. Society of experimental mechanics annual conference, Orlando, FL; June 2008.
[41] Guo Y, Bradshaw RD. Mechanics of time-dependent materials conference, Monterey, CA; March 2008.
[42] Bradshaw RD, Brinson LC. ASME J Eng Mat Tech 1997;119(3):233–41.